Cerâmica, v: 69,(392), 272-277, 2023
ORIGINAL ARTICLE
http://dx.doi.org/10.1590/0366-69132024703923494

Study on the morphological, crystalline, and magnetization effects of Nb_2O_5 addition via high-energy milling in EUROFER chips

R. A. C. Menezes[1], D. P. Gurgel[1], J. H. Araujo[1], U. U. Gomes[1]*
[1]*Federal University of Rio Grande do Norte, Department of Materials Engineering, Natal, RN, Brazil*

Abstract

EUROFER is a reduced-activity ferritic-martensitic steel used in the construction of nuclear fusion reactors. Despite its good properties of mechanical strength, corrosion, creep, and radioactive damage, its maximum working temperature is 500 °C due to microstructural changes that occur above this condition. This study aims to investigate the use of niobium pentoxide (Nb_2O_5) in EUROFER-based alloys through a high-energy milling technique. EUROFER chips were processed in a planetary ball mill with different concentrations of Nb_2O_5 for 10 h. The results showed a reduction of approximately 32% in the particle size distribution of the milled powders compared to pure EUROFER. The X-ray diffraction patterns revealed a decrease solely in the lattice parameters of pure EUROFER and samples containing 3% Nb_2O_5. The addition of Nb_2O_5 also resulted in a reduction in saturation magnetization, and an increase in coercivity and magnetic remanence.
Keywords: EUROFER, niobium pentoxide, powder metallurgy, high-energy milling, magnetic properties.

INTRODUCTION

The 'ITER' (Latin for 'the way') is one of the most ambitious projects in the field of energy worldwide. The largest tokamak ever designed, the ITER, is currently under construction and aims to demonstrate that the energy released through nuclear fusion can be utilized as a source of electricity on a large scale, with zero CO_2 emissions. The anticipated date for achieving its first plasma is 2025 [1]. Throughout this journey, new materials have been developed and refined with the aim of enabling the production of electrical energy from nuclear fusion [2, 3]. One example of such materials is EUROFER steel, which has been specifically designed for use in the tokamak blankets. Its chemical composition has been studied and engineered to exhibit properties such as reduced activation and rapid decay when ionized, as well as a diminished shift in the ductile-to-brittle transition temperature after irradiation [4-9]. Due to its excellent performance in terms of radiation resistance, swelling, high-temperature corrosion resistance, as well as high hardness, tensile strength, and reasonable ductility, the utilization of EUROFER in the ITER project has already been confirmed [10, 11].

However, as steel, EUROFER exhibits inherent flaws when exposed to high temperatures, such as creep, as well as swelling due to neutron and gamma-ray bombardment resulting from nuclear fusion reactions. In light of this scenario, researchers have begun to explore ways to address these issues while preserving the material's existing properties and aiming to enhance its performance and expand its applications. Consequently, studies have shown that yttrium oxide dispersion strengthening (ODS) in this steel has emerged as an intriguing solution to improve these properties [12-15]. It is also known that in recent decades, materials containing niobium (Nb) in their composition have gained prominence due to their special applications in high-tech industries, such as aerospace and nuclear sectors [16]. With Brazil having the largest exploitable reserve globally (~96%) and accounting for approximately 98% of the world's Nb production, it has become the largest producer and exporter of this element [17].

In this context, the objective of this study is to investigate the effect of Nb_2O_5 addition in EUROFER-based alloys using the high-energy milling technique of powder metallurgy (PM) on the morphology and the structural, chemical, and magnetic properties of the resulting powders.

EXPERIMENTAL

The starting material utilized was the EUROFER steel bar (Villares Metals, São Paulo, Brazil), with its composition provided by the company as reported in [7]. The Nb_2O_5 powder (CBMM, Brazil) had a purity level of 99.8%, and an average particle size of 4 μm. Fig. 1a exhibits the ferritic-martensitic microstructure of EUROFER, indicating the martensitic matrix with dispersed ferrite. Fig. 1b shows the X-ray diffraction (XRD) pattern of the as-received sample, in which the experimental data is in agreement with the ICSD file (#102753) and previous reports [18]. The Rietveld method provided the average crystallite size of 53.9 nm, and lattice parameters a=b=c=2.88 Å. The steel bar machining residues were prepared as chips to simulate the machining process using a milling machine

**roberta.cmenezes@hotmail.com*
https://orcid.org/0000-0001-6209-7096

(FUA300, Zema) operating at a cutting speed of 400 rpm, a cutting depth of 0.02 mm, and a feed rate of 23 mm/min. Subsequently, the chips were milled in a planetary mill (Pulverisette 7 Premium Line, Fritsch) using VC131 steel balls. The milling process was conducted in a dry medium with a rotational speed of 400 rpm, and a ball-to-powder mass ratio of 10:1. Four different compositions were tested, namely, 0, 3, 5, and 7 wt% Nb_2O_5, for a duration of 10 h.

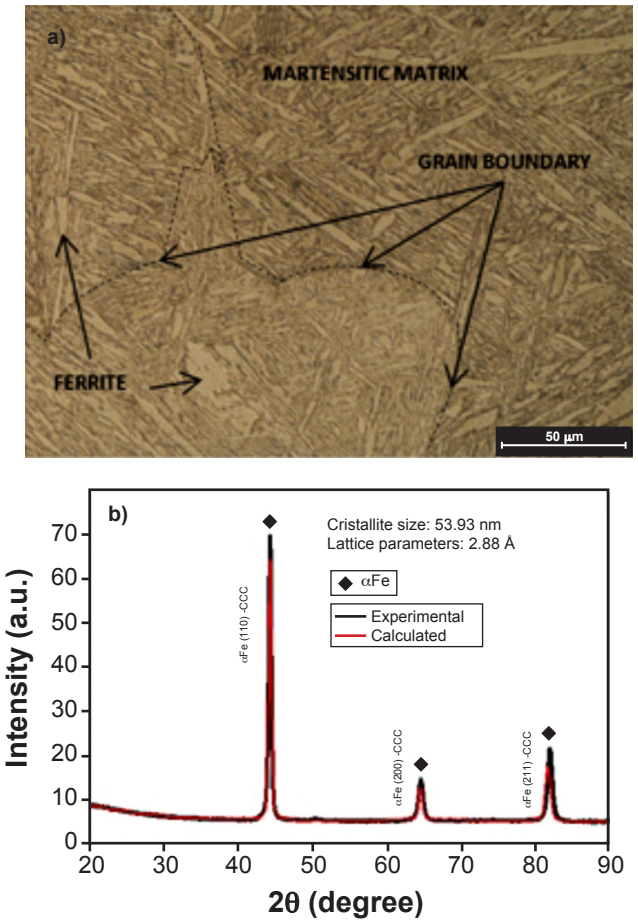

Figure 1: Optical micrograph revealing the ferritic-martensitic microstructure (a) and XRD pattern (b) of the as-received EUROFER bar.

Fig. 2a presents the nodular and agglomerated morphology of Nb_2O_5. Fig. 2b displays the X-ray diffraction (XRD) pattern of Nb_2O_5, where the experimental data agrees with the previous reports by Ding et al. [19] (with lattice parameters a=21.15 Å, b=3.82 Å, c=19.36 Å, and β=119.80°) and the refinement information indicated H-Nb_2O_5. The Rietveld method yielded an average crystallite size of 74.9 nm, and lattice parameters of: a=21.15 Å, b=3.82 Å, c=19.36 Å, and β=119.80°.

Particle size distribution (PSD) analysis was conducted using a laser scattering analyzer (mod. 920, Cilas) in an aqueous medium without dispersants. Scanning electron microscopy with a field emission gun (SEM-FEG, Auriga, Carl Zeiss) was performed. The crystalline structure of the samples was examined using X-ray diffraction (XRD,

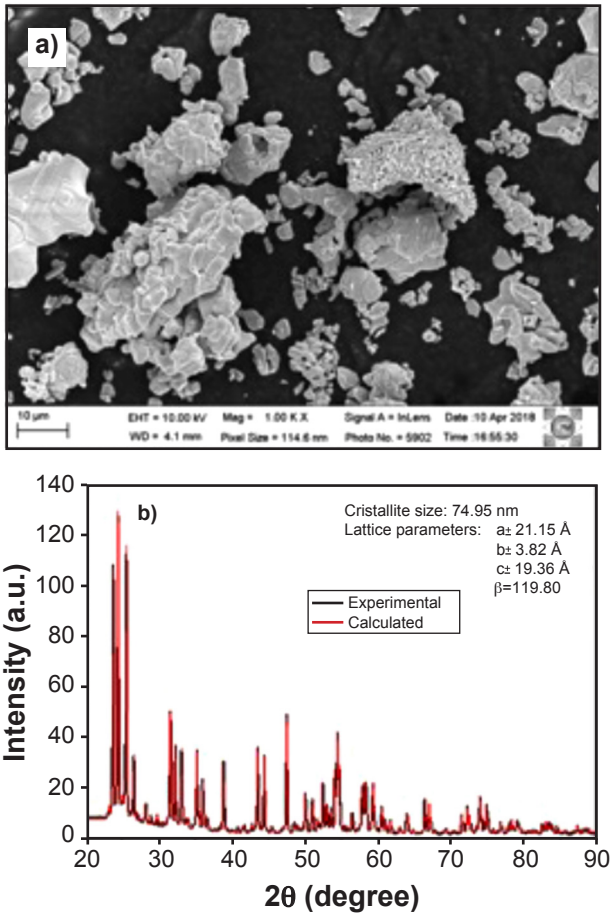

Figure 2: SEM image revealing the nodular and agglomerated morphology (a) and XRD pattern (b) of the as-received Nb_2O_5 sample.

Miniflex-II, Rigaku; CuKα) with a scanning speed of 2 °/min. The XRD measurements covered a 2θ range from 20° to 90° with a step size of 0.01°. The XRD data were refined using MAUD software to determine the grain sizes and lattice parameters of the steel bar and powders. Magnetic properties were characterized using a vibrating sample magnetometer (VSM, mod. 7400, Lakeshore) at room temperature. The maximum applied magnetic field was ±10.0 kOe.

RESULTS AND DISCUSSION

Fig. 3 displays the histograms of particle size distributions, q_3, and cumulative frequency distributions, Q_3 (Figs. 3a, 3c, 3e, and 3g), along with scanning electron microscopy (SEM) micrographs of EUROFER powders with the addition of 0, 3, 5, and 7 wt% Nb_2O_5 powders (Figs. 3b, 3d, 3f, and 3h, respectively) after comminution. In general, the SEM micrographs of the powders exhibited a nodular/irregular morphology [20] with heterogeneity in particle sizes for each sample. The histograms shown in Fig. 3a display a bimodal Gaussian distribution with two density probabilities of normal particle size distributions. The presence of Nb_2O_5 in the milling process (Figs. 3c, 3e, and 3g) tended to reduce this bimodality, resulting in

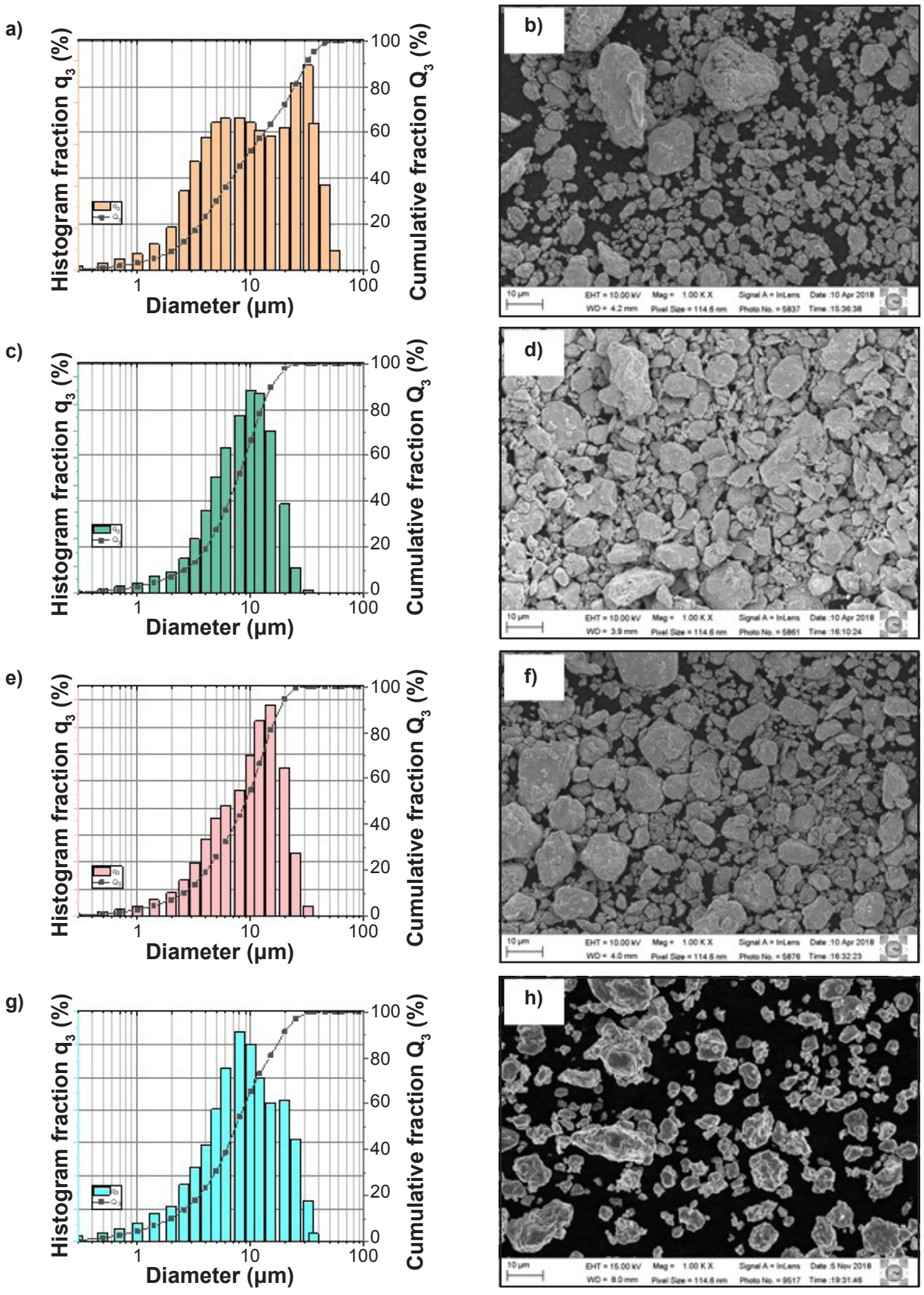

Figure 3: Particle size distribution results (a,c,e,g) and SEM-FEG images (b,d,f,h) of pure EUROFER powder (a,b) and powders with 3 wt% (c,d), 5 wt% (e,f), and 7 wt% (g,h) of Nb_2O_5 milled for 10 h.

density probabilities of normal particle size distributions centered around a single value, as well as a reduction in the particle size distribution. Additionally, in Figs. 3a, 3c, 3e, and 3g, the cumulative frequency curves Q_3 indicate that the variation in Nb_2O_5 composition had little influence on the reduction in particle size distribution of the milled powders containing the oxide. However, examining the D_{50} values, it can be stated that the addition of niobium pentoxide facilitated a reduction in particle sizes by approximately 44% compared to the D_{50} of pure EUROFER powder. These characteristics are favorable for the compaction and sintering of these powders.

In the X-ray diffraction patterns of EUROFER powders with the addition of 0% (Fig. 4a), 3% (Fig. 4b), 5% (Fig. 4c), and 7% (Fig. 4d) Nb_2O_5, the peaks associated with the α-Fe phase with a body-centered cubic (BCC) structure are observed. This indicated that even in the presence of Nb_2O_5, no phase changes occurred during the 10 h milling process. Furthermore, the diffraction profile of Nb_2O_5 was not observed, which suggested either the amorphization of the ceramic during the milling process or the reduction of the oxide and possible incorporation of its elements into the crystalline structure of the steel. However, there was a change in the lattice parameters (a reduction of 0.01 Å, Table I) in the powder with 0 and 3 wt% Nb_2O_5 compared to the lattice parameter of the initial bar. This reduction may be associated with the mechanical alloying process itself, which subjects the milled materials to significant deformations through impacts, compressive forces, and shear, and these effects can be observed in the decrease of the lattice parameters [21]. In the case of milled chips containing 5 and 7 wt% Nb_2O_5, the lattice parameters remained similar to those of the starting material. This preservation of the lattice parameter could be attributed to the formation of a new composition within the steel's solid solution, which effectively maintained the lattice parameter in these materials. Table I provided evidence that, on average, there was a significant reduction of 62% in the crystallite size (approximately 20 nm) of the resulting powders.

Coercivity (H_c), one of the most investigated magnetic parameters in this steel, reflects the pinning strength exerted on the magnetic domain walls. It is highly dependent on the crystallite size (D), internal stresses, and dislocation density (ρ) within the material [22]. For ferritic steels, it is well-known that H_c is proportional to the square root of ρ (H_c α $\rho^{1/2}$) and inversely proportional to D (H_c α 1/D). Studies have shown that H_c for annealed EUROFER up to 800 °C, where there is essentially a reduction in dislocations resulting in relief of internal stresses, is around 5 Oe [23-27]. In Fig. 5, it can be observed that the addition of Nb_2O_5 reduced the saturation magnetization (M_s) of the samples from 193 emu/g (0% Nb_2O_5) to 176 emu/g (7% Nb_2O_5) while increasing the coercivity (H_c) from 69.3 Oe (0% Nb_2O_5) to 84.4 Oe (7% Nb_2O_5). Additionally, the remanent magnetization (M_r) increased from 5.54 emu/g (0% Nb_2O_5) to 7.95 emu/g (7% Nb_2O_5). Generally, this occurs because magnetic measurements are non-destructive in nature and have high sensitivity to detect chemical composition and microstructural variations in ferromagnetic materials. The addition of a second phase (Nb_2O_5) during the milling process not only hinders the random redistribution of magnetic domains, which requires more energy to realign them in a different direction but also may result in chemical composition changes of Nb_2O_5 due to the milling process.

CONCLUSIONS

The present study aimed to contribute to the development of new EUROFER-based alloys with the addition of Nb_2O_5 using powder metallurgy and high-energy milling. From the observation and analysis of the results, the following conclusions can be drawn: i) the results suggested that during the milling process, Nb_2O_5 was decomposed, and Nb was incorporated into the EUROFER alloy (α-Fe); ii) the addition of Nb_2O_5 in the 10 h milling favored the reduction in particle size of the composite powders by approximately 32% compared to pure EUROFER powder; however, the variation in Nb_2O_5 content during milling did not have a significant influence; iii) the morphology of the milled powders exhibited nodular/irregular shapes with particle size heterogeneity for all powders; iv) the average crystallite size of the 10 h milled powders reduced by approximately 62% compared to the initial bar; however, the average crystallite size of the produced powders did not undergo considerable reductions with varying percentages of Nb_2O_5; v) there were changes in the lattice parameters of the milled powders with 5 and 7 wt% Nb_2O_5, suggesting the introduction of atoms into the crystal lattice of α-Fe; vi) the addition of Nb_2O_5 tended to reduce the saturation magnetization of the powders at all milling times, which could be related to a change in the composition of the studied alloy; both the coercivity (H_c) and remanent magnetization (M_r) increased with the addition of the studied oxide and with long milling time.

ACKNOWLEDGMENTS

This study was financed in part by the Coordenação de Aperfeiçoamento de Pessoal de Nível Superior - Brasil (CAPES) - Finance Code 001. The authors would also like to express their sincere gratitude to the School of Engineering of Lorena, University of São Paulo (EEL-USP, Brazil), and the Laboratory of Ceramic Materials and Special Metals (LMCME) at UFRN for their support and facilities throughout this research. Special thanks are extended to Menezes Comércio e Serviços Ltda. for their valuable contributions and collaboration. The authors would also like to acknowledge the Characterization Laboratory for their assistance in conducting various analyses and measurements during the course of this study.

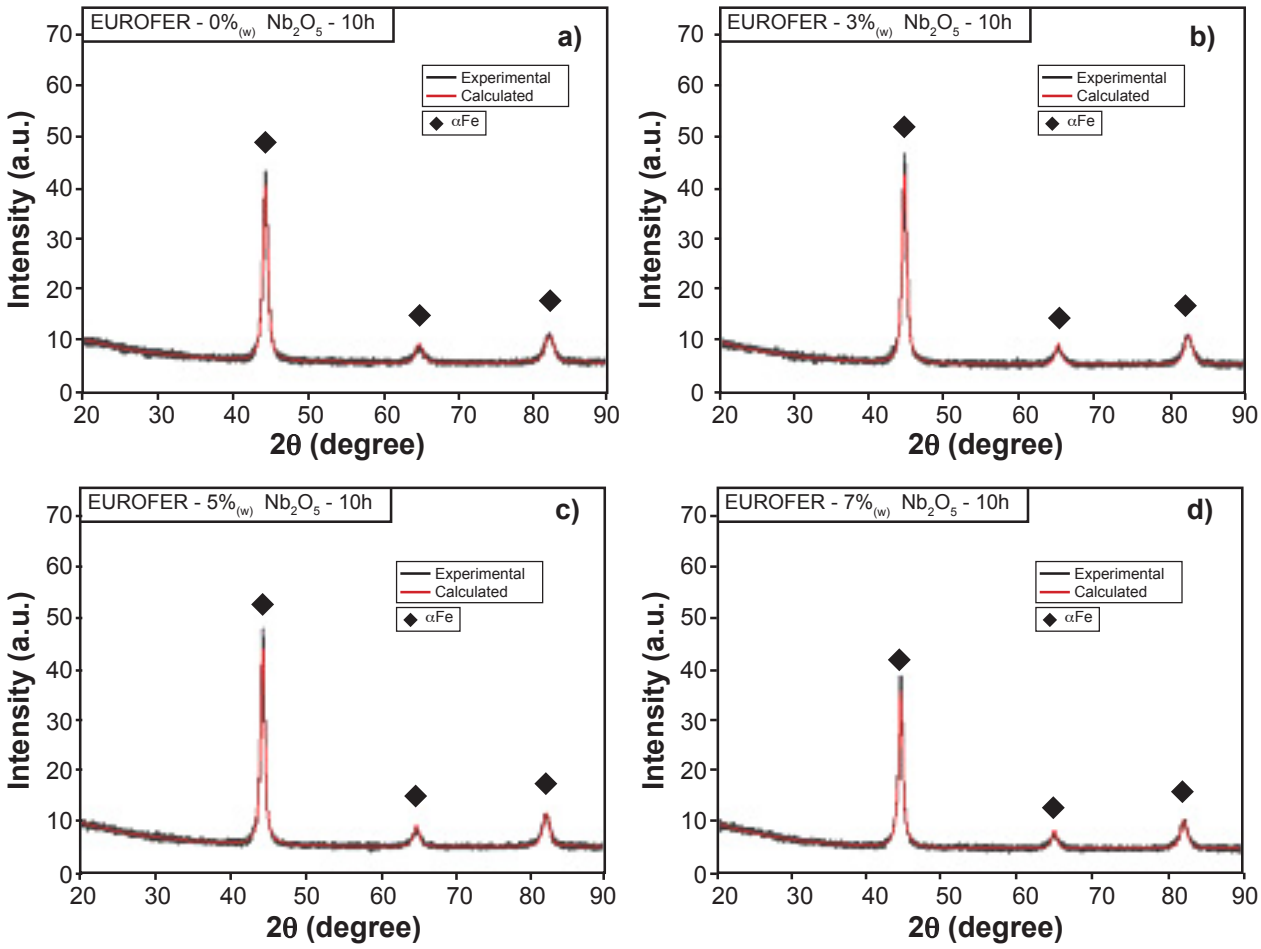

Figure 4: XRD patterns of pure EUROFER powder (a) and EUROFER powders with 3 wt% (b), 5 wt% (c), and 7 wt% (d) of Nb_2O_5 milled for 10 h.

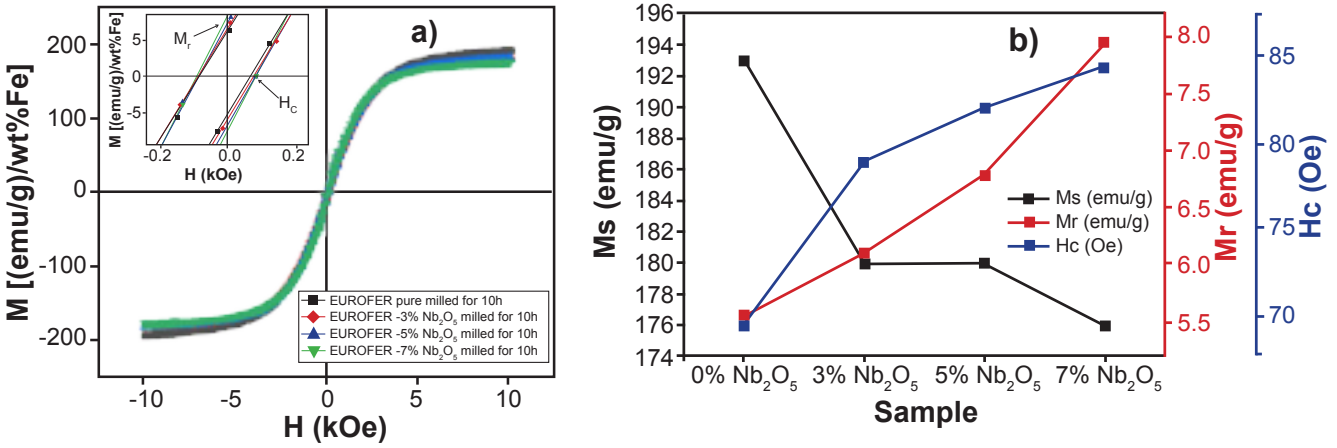

Figure 5: Magnetization curves (a) and values of M_s, M_r, and H_c (b) of pure EUROFER powder and powders with 3, 5, and 7 wt% of Nb_2O_5 milled for 10 h.

Table I - Information from the X-ray diffraction (XRD) refinement of the pure EUROFER powder and the powders with 3, 5, and 7 wt% Nb_2O_5 milled for 10 h (with lattice parameters a=b=c).

Sample	0 wt%	3 wt%	5 wt%	7 wt%
Lattice parameter (Å)	2.87	2.87	2.88	2.88
Crystallite size (nm)	20.3	20.5	20.4	19.7

REFERENCES

[1] ITER, The ITER story, www.iter.org, acc. 15/06/2023.
[2] I. Kuběna, J. Polák, P. Marmy, T. Kruml, Procedia Eng. **74** (2014) 401.
[3] P. Marmy, T. Kruml, J. Nucl. Mater. **377** (2008) 52.
[4] J. Fu, J.C. Brouwer, R.W.A. Hendrikx, I.M. Richardson, M.J.M. Hermans, Mater. Sci. Eng. A **770** (2020) 138568.

[5] R. Lindau, A. Möslang, M. Rieth, M. Klimiankou, E. Materna-Morris, A. Alamo, A.A.F. Tavassoli, C. Cayron, A.M. Lancha, P. Fernandez, N. Baluc, R. Schäublin, E. Diegele, G. Filacchioni, J.W. Rensman, B.V.D. Schaaf, E. Lucon, W. Dietz, Fusion Eng. Des. **75-79** (2005) 989.
[6] G.L. Liu, S.W. Yang, W.T. Han, L.J. Zhou, M.Q. Zhang, J.W. Ding, Y. Dong, F.R. Wan, C.J. Shang, R.D.K. Misra, Mater. Sci. Eng. A **722** (2018) 182.
[7] E. Lucon, P. Benoit, P. Jacquet, E. Diegele, R. Lässer, A. Alamo, R. Coppola, F. Gillemot, P. Jung, A. Lind, S. Messoloras, P. Novosad, R. Lindau, D. Preininger, M. Klimiankou, C. Petersen, M. Rieth, E. Materna-Morris, H.C. Schneider, J.W. Rensman, B. Van Der Schaaf, B.K. Singh, P. Spaetig, Fusion Eng. Des. **81** (2006) 917.
[8] G. Pezzotti, A.A. Porporati, J. Biomed. Opt. **9** (2004) 372.
[9] A.J.O. Zimmermann, H.R.Z. Sandim, A.F. Padilha, REM Rev. Esc. Minas **63** (2010) 287.
[10] L. Forest, J. Aktaa, L.V. Boccaccini, T. Emmerich, B. Eugen-Ghidersa, G. Fondant, A. Froio, A.L. Puma, H. Namburi, H. Neuberger, J. Rey, L. Savoldi, D. Sornin, L. Vala, Fusion Eng. Des. **152** (2020) 111420.
[11] F.A. Hernández, P. Pereslavtsev, G. Zhou, Q. Kang, S. D'Amico, H. Neuberger, L.V. Boccaccini, B. Kiss, G. Nádasi, L. Maqueda, I. Cristescu, I. Moscato, I. Ricapito, F. Cismondi, Fusion Eng. Des. **157** (2020) 111614.
[12] M. Klimiankou, R. Lindau, A. Möslang, J. Nucl. Mater. **367-370** A (2007) 173.
[13] R. Mateus, P.A. Carvalho, D. Nunes, L.C. Alves, N. Franco, J.B. Correia, E. Alves, Fusion Eng. Des. **86** (2011) 2386.
[14] R. Xie, Z. Lu, C. Lu, Z. Li, X. Ding, C. Liu, Fusion Eng. Des. **115** (2017) 67.
[15] J. Fu, J.C. Brouwer, I.M. Richardson, M.J.M. Hermans, Mater. Lett. **256** (2019) 2.
[16] O.F. Lopes, V.R. de Mendonça, F.B.F. Silva, E.C. Paris, C. Ribeiro, Quim. Nova **38** (2014) 106.
[17] H.J. Seer, L.C.D. Moraes, *Nióbio*, RMMG-Codemge, Belo Horizonte (2018).
[18] X. Zhou, Y. Liu, L. Yu, Z. Ma, Q. Guo, Y. Huang, H. Li, Mater. Des. **132** (2017) 158.
[19] H. Ding, Z. Song, H. Zhang, X. Li, Mater. Today Nano **11** (2020) 100082.
[20] U.U. Gomes, *Powders technology: fundamentals and applications*, UFRN Ed. Univ., Natal (1995).
[21] C. Suryanarayana, Prog. Mater. Sci. **46** (2001) 1.
[22] K. Mergia, N. Boukos, J. Nucl. Mater. **373** (2008) 1.
[23] B.D. Cullity, C.D. Graham, *Introduction to magnetic materials*, 2nd ed., Wiley-IEEE Press, Hoboken (2008).
[24] R.A. Renzetti, H.R.Z. Sandim, M.J.R. Sandim, A.D. Santos, A. Möslang, D. Raabe, Mater. Sci. Eng. A **528** (2011) 1442.
[25] M.J.R. Sandim, F.U. Farrão, V.B. Oliveira, E.H. Bredda, A.D. Santos, C.A.M. dos Santos, H.R.Z. Sandim, J. Nucl. Mater. **461** (2015) 265.
[26] M.J.R. Sandim, R.A. Renzetti, C. Bormio-Nunes, H.R.Z. Sandim, Fusion Eng. Des. **126** (2018) 5.
[27] R.A. Raimundo, R.S.S. Reinaldo, N.T. Câmara, C.S. Lourenço, F.A. Costa, D.A. Macedo, U.U. Gomes, M.A. Morales, Ceram. Int. **47** (2021) 984.
(Rec. 23/06/2023, Rev. 25/08/2023, Ac. 19/10/2023)